中國機械工程學刊第四十六卷第四期第 363~376 頁(民國一百一十四年)
Journal of the Chinese Society of Mechanical Engineers, Vol.46, No.4, pp363~376 (2025)

Multi-Objective Optimization for Enhancing Rail E-Clip Design in Fastening Systems

Cheng-Kang Lee*, Yung-Chang Cheng**, Chih-Chiang Lin***, Cheng-Hao Huang****, Chen-Ming Kuo***** and Ming-Yi Hsu******

Keywords： rail fastening system, rail e-clip, von Mises stress, fatigue safety factor, uniform design, Kriging interpolation, Sobol sensitivity analysis.

ABSTRACT

This study focuses on improving the fatigue safety and structural strength of a rail e-clip in fastening systems under impact, fatigue, and static loads by employing advanced optimization techniques. Using the EN 13146-1, EN 13146-2, and EN 13146-3 testing standards, von Mises stress in the rail e-clip is evaluated via simulations performed in ANSYS/Workbench. Additionally, EN 13146-4 testing simulations assess the fatigue safety factor. The multi-objective optimization problem is solved using an integrated approach combining the uniform design of experiments methodology, Kriging interpolation, entropy weighting method, grey relational analysis, and the genetic algorithm, leading to an optimal design. The improved design shows reductions in von Mises stress of 9.9%, 22.12%, and 28.6% for the EN 13146-1, EN 13146-2, and EN 13146-3 testing simulations, respectively, compared to the original model. Meanwhile, the EN 13146-4 testing simulation shows a 29.8% improvement in the fatigue safety factor, which rises to 6.18. Thus, the structural strength and fatigue performance of the rail e-clip are significantly improved. Finally, the impact of each design variable on the objective functions is determined using Sobol sensitivity analysis. According to the sensitivity results, the diameter of the rail clip has a significant impact on most objective functions.

Paper Received October, 2024. Revised December, 2024. Accepted February, 2025. Author for Correspondence: Yung-Chang Cheng.

* *Professor, Department of Industrial Engineering and Management, Cheng Shiu University, Kaohsiung, Taiwan 833301, ROC.*

** *Professor, Department of Mechatronics Engineering, National Kaohsiung University of Science and Technology, Kaohsiung, Taiwan 824005, ROC.*

*** *Assistant Professor, Department of Civil Engineering, National Kaohsiung University of Science and Technology, Kaohsiung, Taiwan 807618, ROC.*

**** *Assistant Professor, Department of Vehicle Engineering, National Taipei University of Technology, Taipei, Taiwan 10608, ROC.*

***** *Professor, Department of Civil Engineering, National Cheng Kung University, Tainan, Taiwan 701401, ROC.*

****** *Graduated Student, Department of Mechatronic Engineering, National Kaohsiung University of Science and Technology, Kaohsiung, Taiwan 824005, ROC.*

INTRODUCTION

The railway vehicle is widely regarded as the best way to transport people and goods efficiently. It's important to consider stability and safety when designing the rail and fastening system. The rail fastening system is crucial for connecting parts and keeping the rail aligned, preventing sideways movement for a smoother ride and less chance of derailment.

The structural stress within fastening systems has been extensively studied through finite element analysis (FEA) by several researchers (Mohammadzadeh et al., 2014; Ferreo et al., 2019; El-sayed et al., 2021; Hong et al., 2018; Kim et al., 2021; Cheng et al., 2021). Mohammadzadeh et al. (2014) used FEA software to conduct stress analysis on SKL14 Vossloh fastening clips under various train speeds and axle loads. Ferreo et al. (2019) combined experimental methods with FEA to study the structural integrity of the elastic clip fastening mechanism for the SKL-1. El-sayed et al. (2021) employed a three-dimensional finite element railway model to investigate the structural stress in railway concrete sleepers and fastening systems. Hong et al. (2018) assessed the fatigue safety and predictability of e-clip fastening systems under cyclic loading using ABAQUS software. Kim et al. (2021) investigated the structural stress and fatigue performance of KR-type rail clips using finite element analysis software. Meanwhile, Cheng et al. (2021) analyzed the von Mises stress and fatigue safety factor of the SKD type rail clip fastening system with the aid of ANSYS/Workbench software.

The fatigue analysis and testing of rail

fastening systems are important research areas that have been extensively studied by several researchers (Yan et al., 2023; Kim et al., 2022; Choi and Kim, 2020; Park et al., 2019; Fang et al., 2023; Xiao et al., 2017; Liu et al., 2021). Yan et al. (2023) investigated the static-dynamic characteristics and the mechanism of fatigue failure induced by vibration in railway fastening clips using finite element analysis. Kim et al. (2022) conducted experiments to identify tension clamp fractures and performed reliability analyses on the fatigue failure of such fractures. Choi and Kim (2020) utilized numerical simulations to investigate the failure mechanism of rail fastening systems. Park et al. (2019) investigated the fatigue strengths, strains, and displacements of SKL15 and SKLB15 elastic clip fastening systems through a combination of experimental measurements and FEA software. Fang et al. (2023) evaluated the fatigue performance of the SPS9 spring steel commonly used in fastening springs and included a sensitivity analysis to identify factors influencing shape change in the material. Xiao et al. (2017) studied fastener fractures and proposed effective repair methods using ABAQUS software. Liu et al. (2021) assessed the maximum strain and minimum fatigue life of rail clips under dynamic cyclic loading using FEA techniques.

Multiple studies have investigated the stress and fatigue life of rail e-clips (Hong et al., 2018; Xiao et al., 2017). However, there has been no specific analysis of the impact load testing of the rail e-clip fastening system. Furthermore, there is a lack of research on optimizing the geometry design of the rail e-clip in the fastening system. Improving the strength and fatigue safety of a rail clip is crucial. This research introduces a new approach using multi-objective optimization to create an optimal rail e-clip design. This design considers static, impact, and fatigue simulations, comprehensively addressing all these factors.

A series of simulation experiments were systematically organized using the uniform design (UD) approach. Finite element models were constructed to simulate various scenarios within the rail e-clip fastening system, such as longitudinal rail restraint, torsional resistance, impact load, and repetitive load, in accordance with testing standards EN 13146-1, EN 13146-2, EN 13146-3, and EN 13146-4. ANSYS/Workbench software was used to evaluate the distributions of von Mises stress (VMS) and fatigue safety factors (SF) for the rail e-clip. Surrogate models for minimal SF and maximum VMS were created using the Kriging interpolation approach. These models were integrated into a single objective, the grey relation grade, using grey relational analysis (GRA), Kriging interpolation (KGI), and entropy weighting analysis (EWA). The optimal design model for the rail e-clip within the fastening system was developed using genetic algorithm (GA). According to numerical data, the rail e-clip's strength and fatigue safety were significantly improved by using this innovative multi-objective optimization technique. Additionally, the Sobol sensitivity analysis was used to thoroughly evaluate the impact of control variables on every objective function, yielding insightful results.

MODELLING AND FINITE ELEMENT ANALYSIS

Components in E-Clip Fastening System

The e-clip fastening model (Figure 1) used within the railway track system with various components such as the e-clip itself, a gauge plate, a rail pad, and a sleeper. Figure 1 shows a simplified version of the e-clip fastening system. The e-type rail clip has been widely utilized in both conventional railway systems.

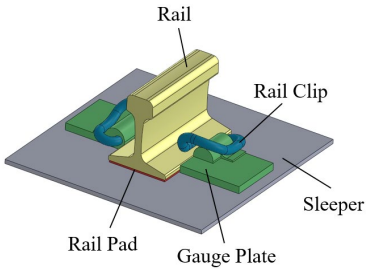

Fig. 1 Full components in the rail fastening system.

The Fastening System Testing Standard

It is crucial to conduct a series of comprehensive examinations, including tensile, bending, impact, and dynamic fatigue assessments, to ensure the safety and reliability of the fastening system. All tests must adhere to the EN 13146 standard for fastening system testing. The details of the EN 13146-1 (2002) test, which focuses on the evaluation of longitudinal rail restraint through simulation, are presented in Figure 2(a). Two fastening methods are utilized to secure the rail during the EN 13146-1 test, while applying a tensile force of 2.5 kN to one end of the rail and firmly attaching the sleeper to the ground. Figure 2 illustrates the test methods employed in the current investigation.

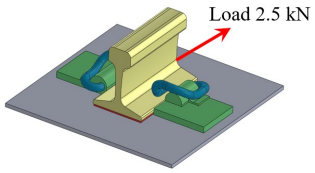

(a)

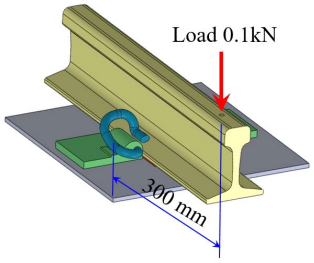

(b)

Fig. 2 Simulation setup in a rail fastening system for (a) EN 13146-1, (b) EN 13146-2 standard.

In Figure 2(b), the torsional resistance test in EN 13146-2 standard (EN 13146, 2002) is shown. In this test, the length of the rail is greater than the width of the sleeper. The sleeper is firmly attached to the ground, and a force of 0.1 kN is applied to the rail 300 mm away from the gauge plate.

The simulation showing the influence of impact load testing in EN 13146-3 (EN 13146, 2002) is presented in Figure 3. According to this test guideline, a concentrated force F = 50 kN is applied to the upper section of the rail, vertically aligned with the rail's direction, as shown in Figure 3(a). The periodic nature of the impact force, lasting for 5 ms, is depicted in Figure 3(b).

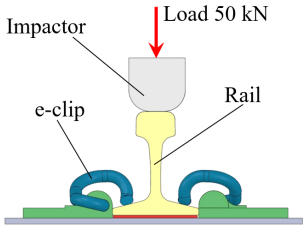

(a)

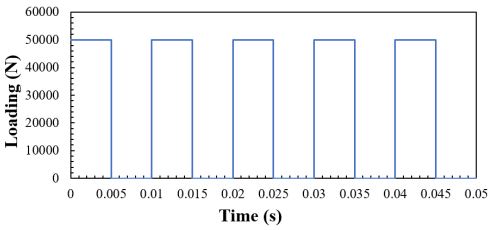

(b)

Fig. 3 (a) Simulation setup in a rail fastening system for EN 13146-3 testing technique (b) the periodic of the impact load.

In Figure 4, a simulation illustrates the impact of repetitive load testing as outlined in EN 13146-4 (EN 13146, 2002). Following the recommendations in EN 13481-5 (2012), the dynamic stiffness of the assembly at low frequencies is determined. As a result, the rail and fastening system are positioned on the sleeper at a 26-degree angle, using a combination of the methods from EN 13146-4 and EN 13481-5, as depicted in Figure 4. Additionally, the rail undergoes cycles of compressive repeated loads of 65 kN at a frequency of 5 Hz.

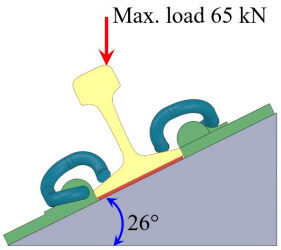

Fig. 4 Simulation setup in a rail fastening system for EN 13146-4 testing technique.

Finite Element Simulation for Static and Fatigue Testing

In Figure 5, the rail fastening e-clip model created using SolidWorks software is displayed. ANSYS/Workbench is used for pre-processing, where key parameters such as element size, boundary conditions, mechanical characteristics, and contact configurations are specified. The rail clip is made from 38Si7 material, with mechanical properties based on JIS 60 standards. The traditional railway and MRT systems use the e-clip fastening model. The mechanical characteristics of components, including the screw, guide plate, and rail pad, are listed in Table 1 (Mohammadzadeh et al., 2014; Ferreo et al., 2019; Hasap et al., 2018) and used in the finite element analysis procedure. The selection of maximum von Mises stress as the primary indicator for convergence analysis is based on the distortion energy theory, which is widely accepted in mechanical design. For analysis purposes, the sleeper is treated as a rigid body. The flat feet of the e-clip apply a clamp force of 13 kN, making contact with the rail, as shown in Figure 5 (Iqbal et al., 2024). Using ANSYS/Workbench software, the fatigue safety of the rail clip is analyzed, considering the SN curve specific to the rail e-clip, depicted in Figure 6 (Ferreo et al., 2019).

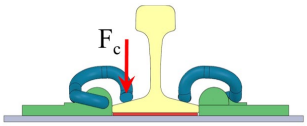

Fig. 5 The clamp force between the clip and rail.

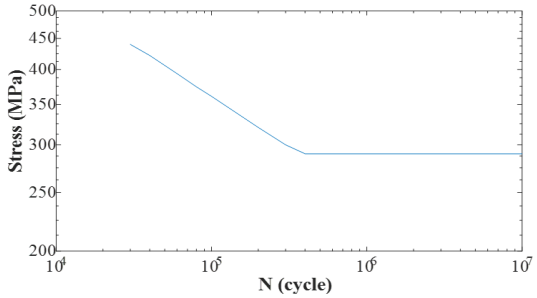

Fig. 6 SN curve of the rail e-clip.

We will use ANSYS/Workbench software to conduct simulations following EN 13146-1, EN 13146-2, and EN 13146-3 testing standards. Our goal is to calculate and visually represent the distribution of VMS within the rail e-clip. The boundary condition for the fastening system is illustrated in Figure 7(a) in compliance with the longitudinal restraint testing standard outlined in EN 13146-1. In this study, we will apply boundary conditions to the two components, treating them as automatic and frictional contact interfaces, while maintaining a coefficient of friction set at 0.2 (Ferreo et al., 2019).

It is widely recognized that the size of the elements directly influences the results of finite element analysis. Conducting a mesh convergence analysis of the rail e-clip model is crucial for enhancing analysis accuracy. In Figure 7(b), it is evident that an element size of 2.5 mm yields optimal results, as the maximum von Mises stress (VMS) converges significantly. This trend becomes apparent when the element size decreases below 2.4 mm, with the VMS difference remaining within 5%. Upon examining the VMS distribution in the rail e-clip in Figure 7(c), it is observed that the highest value is 15.99 MPa.

In order to conduct torsional resistance testing according to EN 13146-2 standards, the rail e-clip is analyzed using verified finite elements, as depicted in Figure 8(a). When the element size is reduced to less than 2.1 mm, there is a noticeable convergence of the maximum VMS in the rail e-clip, as shown in Figure 8(b). An optimal element size of 2.5 mm is identified, with a VMS difference of less than 5% compared to the smaller size. The VMS distribution within the rail e-clip is illustrated in Figure 8(c), showing the highest value at 6.42 MPa.

In the impact loads testing simulation, automatic contact with friction between components is established, as seen in Figure 9(a). The rail e-clip shows a significant convergence of maximum VMS as the element size decreases to below 2.2 mm, as shown in Figure 9(b). This confirms the choice of an improved element size of 2.5 mm, with a VMS difference of less than 5% compared to the smaller size. Figure 9(c) displays the VMS distribution within the rail e-clip, with the highest value recorded at 18.42 MPa.

In ANSYS/Workbench software, EN 13146-4 testing simulations are used to evaluate and display SF distribution in the rail e-clip. Meshing is done with verified finite elements for EN 13146-4 repetitive load testing simulation. Contact interactions between components are modeled, as shown in Figure 10(a). An optimal element size of 2.5 mm is chosen for fatigue analysis, supported by the convergence of minimum SF as the element size decreases below 2.4 mm, as shown in Figure 10(b). The difference in SF between these sizes remains within a 5% range. The lowest SF recorded within the rail e-clip is 4.76, as depicted in Figure 10(c).

In Figures 8(c), 9(c), and 10(c), the maximum von Mises stress and minimum fatigue safety factor occurs at the ends of the e-clip. The reason why the maximum equivalent stress and the minimum safety factor occur at the end of the fastener is that this part is in close contact with the rail, and the contact force with the rail is the largest here.

Table 1. Properties of the e-clip fastening system's mechanical characteristic.

Part	Material	Property	Value
e-clip	38Si7 steel	Young's Modulus (GPa)	205
		Poisson's Ratio	0.3
		Density (kg/m^3)	7800
Rail	JIS E 1101-2001	Young's Modulus (GPa)	206
		Poisson's Ratio	0.3
		Density (kg/m^3)	7845
Bolt with washer	S35C	Young's Modulus (GPa)	206
		Poisson's Ratio	0.3
		Density (kg/m^3)	7800
Gauge plate	JIS E 1101-2001	Young's Modulus (GPa)	206
		Poisson's Ratio	0.3
		Density (kg/m^3)	7845
Rail pad	EVA	Young's Modulus (GPa)	20
		Poisson's Ratio	0.4
		Density (kg/m^3)	950

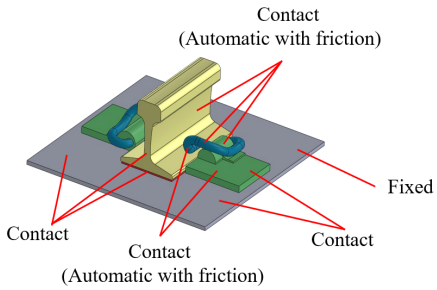

(a)

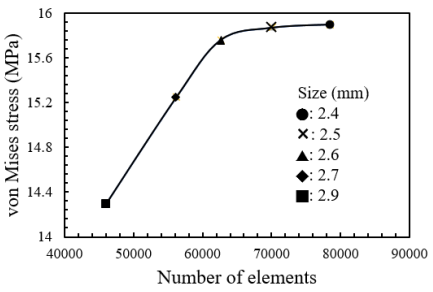

(b)

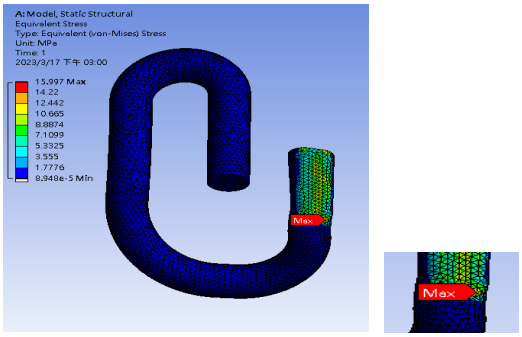

(c)

Fig. 7 (a) The setting of boundary conditions in the finite element model, (b) the convergent analysis curve for elements, (c) the von Mises stress distribution for a rail e-clip under the EN 13146-1 testing simulation.

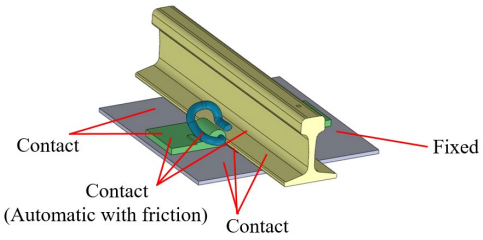

(a)

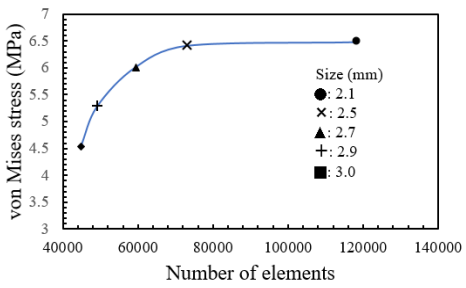

(b)

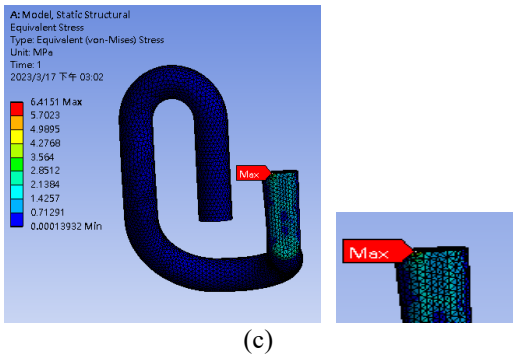

(c)

Fig. 8 (a) The setting of boundary conditions in the finite element model, (b) the convergent analysis curve for elements, (c) the von Mises stress distribution for a rail e-clip under the EN 13146-2 testing simulation.

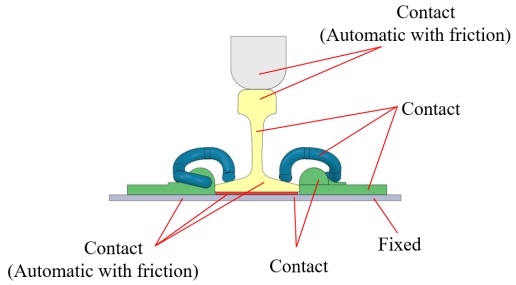

(a)

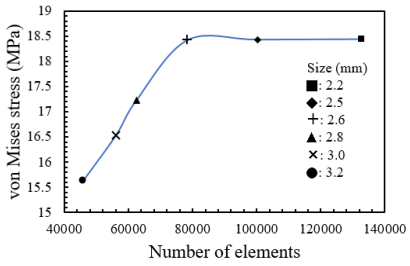

(b)

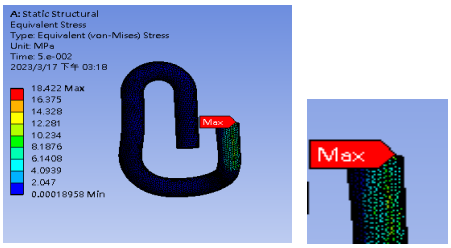

(c)

Fig. 9 (a) The setting of boundary conditions in the finite element model, (b) the convergent analysis curve for elements, (c) the von Mises stress distribution for a rail e-clip under the EN 13146-3 testing simulation.

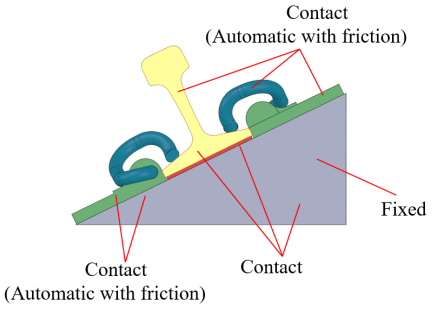

(a)

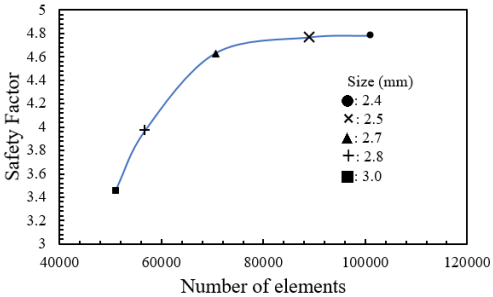

(b)

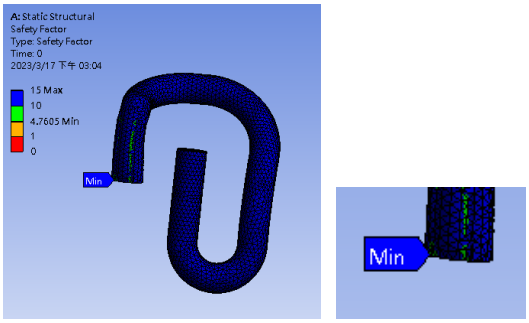

(c)

Fig. 10 (a) The setting of boundary conditions in the finite element model, (b) the convergent analysis curve for elements, (c) the fatigue safety factor distribution for a rail e-clip under the EN 13146-4 testing simulation.

OPTIMIZATION METHODOLOGY

Uniform Design of Experiment

Uniform design, proposed by professors Fang and Wang (1994), is applied in this paper to design a series of experiments. In a continuous design space, design points are infinite and evaluation of all design points is impossible. Uniform design helps the selection of a set of sample points from the design space. The selected sample points are scattered uniformly in the design space. Uniform design has been successfully applied in various fields such as chemistry and chemical engineering, quality engineering, system engineering, and computer sciences.

In this study, we apply uniform design to generate a set of sampling points that are uniformly distributed in the design space. After evaluating performance measures on each sampling point, we still cannot optimize the system since we just get the values of performance measure on the discrete sampling points. The succeeding step is to construct a continuous response surface model based on the discrete results of sampling points. The main features of uniform design are described in Fang and Wang (1994). Suppose a problem has n factors and each factor has q levels. The uniform design selects q combinations out of q^n possible combinations, such that these combinations are uniformly scattered over the space of all possible combinations. Therefore, the uniform design (UD) table can be expressed as $U_q\left(q^n\right)$. If the control factor of the real problem is less than the factors n, the use table will be applied to determined the column numbers in UD table. Then, the suitable UD table for the research topic is finally created.

Grey Relation Analysis

Grey Relational Analysis (GRA) is based on Deng's Grey system theory (1982) and is commonly used to measure the relationship between sequences using a grey relational grade. GRA consolidates multiple performance characteristics into a single value, which is helpful for optimization problems (Shakeri et al., 2022; Huang and Lin, 2009; Muthana and Ku-Mahamud, 2023). The process begins by normalizing input data and calculating coefficients for GRA. The second step involves determining the grey relational coefficients, and the third step involves determining the grey relational grades. In the third step, an entropy weighting analysis is used to determine the weights of sub-objective functions. The procedure for GRA is outlined by Huang and Lin (2009).

Step 1. Data normalization

Before calculating the grey relational coefficients, it is necessary to organize the input and output data. Let $\max_{\forall j} u_i(j)$ represent the maximum value of $u_i(j)$ for the jth response and $\min_{\forall j} u_i(j)$ represent the minimum value of $u_i(j)$ for the jth response. Three types of data processing are employed:

(1) larger-the-better attributes

$$u_i^*(j)=\frac{u_i(j)-\min_{\forall j} u_i(j)}{\max_{\forall j} u_i(j)-\min_{\forall j} u_i(j)} \tag{1}$$

(2) smaller-the-better attributes

$$u_i^*(j)=\frac{\max_{\forall j} u_i(j)-u_i(j)}{\max_{\forall j} u_i(j)-\min_{\forall j} u_i(j)} \tag{2}$$

(3) nominal-the-best attributes

$$u_i^*(j)=1-\frac{\left|u_i(j)-u_{ob}(j)\right|}{max\left[\max_{\forall j} u_i(j)-u_{ob}(j),\ u_{ob}(j)-\min_{\forall j} u_i(j)\right]} \tag{3}$$

where $u_{ob}(j)$ is the objective value of entity j.

Step 2. Determining the grey relational coefficients evaluation

If $u_0=\left[u_0(1),\ u_0(2),\ \cdots,\ u_0(j),\ \cdots,\ u_0(k)\right]$ is the referential series with k entities of $u_1,\ u_2,\ \cdots,\ u_N$, then, $u_i=\left[u_i(1),\ u_i(2),\ \cdots,\ u_i(j),\ \cdots,\ u_i(k)\right]$. The grey relational coefficient $\gamma_{0i}(j)$ between the series u_i and the referential series u_0 at the j-the entity is defined as:

$$\gamma_{0i}(j)=\frac{\Delta\min+\Delta\max}{\Delta_{0i}(j)+\Delta\max} \tag{4}$$

where, $\Delta_{0i}(j)=\left|u_0(j)-u_i(j)\right|$ and it means the difference of the absolute value between $u_0(j)$ and $u_i(j)$. $\Delta\max=\max_{\forall j}\Delta_{0i}(j)$ and it denotes the maximum value of $\Delta_{0i}(j)$. $\Delta\min=\min_{\forall j}\Delta_{0i}(j)$ and it denotes the minimum value of $\Delta_{0i}(j)$.

Step 3. Calculating the grey relational grade

The grey relation coefficients $\gamma_{0i}(j)$ are determined in Step 2, and the grey relational grade for a series is expressed as:

$$\Gamma_{0i}=\sum_{j=1}^{k}W_j\gamma_{0i}(j) \tag{5}$$

where, the weight of attribute j, denoted as W_j, depends on the judgment of decision-makers or the geometry of the research structure. The sum of all weights equals one. In this study, the weight, W_j, is calculated from the entropy weight analysis, which is detailed in the next section.

Entropy Weighting Analysis

The Entropy method, based on probability theory, quantifies the uncertainty in information. Through the entropy weighting analysis (EWA) method, one can assess the information conveyed by each attribute and compute their relative weights. EWA method has found extensive applications in economics, engineering, and information science, among other fields (Wu et al., 2022; Vatansever and Akgul, 2018; Ayşegül and Esra, 2017).

Entropy weight analysis is a powerful method for determining the weight of an index in a decision-making system that incorporates multiple criteria. This four-step process has been referenced by some articles (Ayşegül and Esra, 2017; Vatansever and Akgűl, 2018).

Step 1. Constructing the decision matrix

A set of alternatives $\mathbf{A}=\left[A_i\right]$ compared with respect to a set of criteria $\mathbf{C}=\left[C_j\right]$ so the $n\times m$ decision matrix $\mathbf{Z}$ is evaluated as:

$$\mathbf{Z}=\left[z_{ij}\right]=\begin{bmatrix} z_{11} & z_{12} & \cdots & z_{1m} \\ z_{21} & z_{22} & \cdots & z_{2m} \\ \vdots & \vdots & \ddots & \vdots \\ z_{n1} & z_{n2} & \cdots & z_{nm} \end{bmatrix} \tag{6}$$

where z_{ij} is a crisp value that represents the performance rating for each alternative A_i, with regard to each criterion C_j. The subscripts in Equation (6) are $i=1,2,\cdots,n$ and $j=1,2,\cdots,m$.

Step 2. Decision matrix normalization

To calculate objective weights using entropy, the decision matrix in Equation (6) is normalized for each criterion C_j as follows:

$$p_{ij}=\frac{z_{ij}}{\sum_{p=1}^{n}z_{pj}},\quad i=1,2,\cdots,n \tag{7}$$

The normalized decision matrix is:

$$\mathbf{P}=\left[p_{ij}\right]=\begin{bmatrix} p_{11} & p_{12} & \cdots & p_{1m} \\ p_{21} & p_{22} & \cdots & p_{2m} \\ \vdots & \vdots & \ddots & \vdots \\ p_{n1} & p_{n2} & \cdots & p_{nm} \end{bmatrix} \tag{8}$$

Step 3. Calculating entropy

The entropy value for each index is calculated as:

$$e_j=-\frac{\sum_{i=1}^{n}p_{ij}\ell n\left(p_{ij}\right)}{\ell n(n)} \tag{9}$$

where $1/\ell n(n)$ is a constant that guarantees $0<e_j<1$.

Step 4. Calculating entropy weights

The objective entropy weights W_j for each criterion C_j are calculated as:

$$W_j=\frac{1-e_j}{\sum_{k=1}^{m}(1-e_k)} \tag{10}$$

In Equation (10), $\left(1-e_j\right)$ denotes the degree of divergence in the average intrinsic information that is contained in each criterion C_j.

Kriging Interpolation

Due to the complexity of the rail fastening system, it is challenging to establish direct or indirect relationships between inputs and outputs using explicit or implicit functions. In order to develop meaningful equations for these connections, a statistical surrogate model was utilized. For this study, Kriging, a commonly employed method in engineering research, was selected to accommodate system noise factors. Each objective function is depicted by a Kriging surrogate (KGS) model, constructed using specific simulation data points from the UD dataset.

For a Kriging surrogate model with a zero-order regression function and a Gaussian correlation function, the Kriging surrogate model $y_s(\boldsymbol{x})$ of the unknown response function $y(\boldsymbol{x})$ can be represented by the following equation: (McLeana et al., 2006; Simpson and Mistree, 2001; Cheng and Wu, 2015)

$$y_s(\boldsymbol{x}) = \beta + \boldsymbol{r}^T(\boldsymbol{x})\mathbf{R}^{-1}(\boldsymbol{Y} - \boldsymbol{F}\beta) \quad (11)$$

$\boldsymbol{x} = \{x_1, x_2, \ldots, x_p\}$ is a vector formed by unknown input variables and p is the number of unknown input variables. $\boldsymbol{r}(\boldsymbol{x})$ is a vector of length n and is the function of unknown input variables. $\boldsymbol{r}(\boldsymbol{x})$ is determined by

$$\boldsymbol{r}(\boldsymbol{x}) = \left\{R_c(\boldsymbol{x}, \boldsymbol{x}_1),\ R_c(\boldsymbol{x}, \boldsymbol{x}_2), \cdots,\ R_c(\boldsymbol{x}, \boldsymbol{x}_n)\right\}^T \quad (12)$$

Where

$$R_c(\boldsymbol{x}, \boldsymbol{x}_i) = \prod_{m=1}^{p} Exp\left[-\theta_m (x_m - x_{im})^2\right], i = 1, 2, \cdots, n \quad (13a)$$

$$\boldsymbol{x}_i = \{x_{i1}, x_{i2}, \cdots, x_{ip}\}, i = 1, 2, \cdots, n \quad (13b)$$

$$\boldsymbol{x} = \{x_1, x_2, \ldots, x_p\} \quad (13c)$$

$\boldsymbol{Y} = \{y_1, y_2, \ldots, y_n\}^T$ is a known response vector of unknown function and n is the number of experimental points. $\boldsymbol{F}$ is a known column vector of length n that is filled with ones. $\mathbf{R} = \left[R_{ij}\right]_{n \times n}$ is a known square matrix and is determined by

$$R_{ij} = \prod_{m=1}^{p} Exp\left[-\theta_m (x_{im} - x_{jm})^2\right], \quad i = 1, 2, \cdots, n, j = 1, 2, \cdots, n \quad (14)$$

β is a known constant and is determined by

$$\beta = \left(\boldsymbol{F}^T \mathbf{R}^{-1} \boldsymbol{F}\right)^{-1} \boldsymbol{F}^T \mathbf{R}^{-1} \boldsymbol{Y} \quad (15)$$

The Kriging surrogate model for each objective function is constructed as follows using the mathematical models in Equations (11) to (15). In Equation (14), θ is an important coefficient in the Kriging interpolation. The θ value is related to the error between the Kriging function value and the real analysis value in UD table. This error is used as the objective function. The θ value can be obtained through the calculation of the genetic algorithm after minimizing the error. Then, a response surface consistent with the results in the UD table can be established.

RESULTS OF IMPROVEMENT DESIGN

Design of Experiment Analysis and Results

The four main characteristics of the rail e-clip significantly impact the experimental indicators and are essential for improvement. Figure 11 illustrates the primary design parameters related to the rail e-clip, while Table 2 lists these four control factors. This study focuses on four parameters—L1, L2, L3, and d—all of which serve as control factors to examine how the dimensions of the rail e-clip geometry influence VMS and SF. Table 2 specifies the designed range for each control factor.

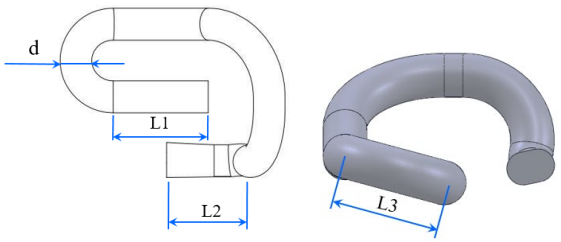

Fig. 11 Four control factors for the rail e-clip.

Table 2. The designed range values for four system control factors.

Control factor	Notation	Lower bound (mm)	Baseline value(mm)	Upper bound (mm)
Length of the first foot part	L1	54	60	66
Length of the second foot part	L2	36	40	44
Distance between the first foot and middle part	L3	42.3	47	51.7
The diameter of the rail clip	d	18	20	22

Every control factor in this study is continuous, not discrete. To conduct simulation experiments for these control parameters, a UD approach is employed. According to Fang and Wang (1994), the UD table utilized in this investigation is $U_{16}^*(16^{12})$ from Fang and Wang (1994), which produces uniform experiments. It contains 16 isometric values for each control component within the given lower and upper constraints. Since the rail e-clip model in this study has four control factors, columns 1, 4, 5, and 6 must be used according to the use table of $U_{16}^*(16^{12})$ described in Fang and Wang (1994). Therefore, the uniform table $U_{16}^*(16^4)$ with four control factors has been used. The uniform experiments generated using $U_{16}^*(16^4)$ this approach are shown in Table 3(a) based on the design space in Table 2.

SolidWorks software is used to create 3D models for each rail e-clip design in simulation experiments. Finite element methods are employed to calculate the maximum VMS and minimum SF, as explained in section 2.3. These experiments yield four objective functions: ST1, ST2, ST3, and SF, which are outlined in Table 3(b). ST1 represents the maximum VMS during EN 13146-1 longitudinal restraint testing, ST2 during EN 13146-2 torsional resistance testing, and ST3 during EN 13146-3 impact load testing. SF indicates the minimum fatigue safety factor observed in EN 13146-4 repetitive load testing simulation. Comparing with analysis results from the basic design model, the

improvement rates of each simulation experiment for ST1, ST2, ST3, and SF are determined and shown in Table 3(c). For ST1, ST2, and ST3, the derivation process of improvement rate is: (basic design value – experimental value)/(basic design value)×100%. For SF, the derivation process of improvement rate is: (experimental value – basic design value)/(basic design value)×100%.

In the first experiment for EN 13146-1 longitudinal restraint testing simulation, the maximum VMS decreased to 14.84 MPa when using a uniform design of experiment. Similarly, in the 6th experiment for EN 13146-2 torsional resistance testing, the maximum VMS decreased to 5.00 MPa. Likewise, in the 16th experiment for EN 13146-3 impact load testing, the maximum VMS dropped to 14.01 MPa. This trend continued in the 6th experiment, where the minimum SF during EN 13146-4 repetitive load testing simulation rose to 6.12. These FEA results are shown in Figure 12. Due to rail e-clips enduring recurring and dynamic loads, the focus is on ensuring adequate fatigue safety rather than static load testing. Thus, the improved version of uniform design outcomes in Table 3(c) is labeled as the 6th experiment. However, it's important to note that the maximum VMS and minimum SF for each test simulation are determined separately. The subsequent phase uses a multi-objective optimization approach to identify the final optimal design due to the challenge of selecting the definitive upgraded design.

Table 3. The uniform design of experiment (a) parameters, (b) results and (c) improvements for uniform table $U_{16}^{*}\left(16^{4}\right)$.

(a)

Experiment No.	L1 (mm)	L2 (mm)	L3 (mm)	d (mm)
1	54.00	38.13	45.43	19.87
2	54.80	40.80	49.19	22.00
3	55.60	43.47	42.30	19.60
4	56.40	37.07	46.06	21.73
5	57.20	39.73	49.82	19.33
6	58.00	42.40	42.93	21.47
7	58.80	36.00	46.69	19.07
8	59.60	38.67	50.45	21.20
9	60.40	41.33	43.55	18.80
10	61.20	44.00	47.31	20.93
11	62.00	37.60	51.07	18.53
12	62.80	40.27	44.18	20.67
13	63.60	42.93	47.94	18.27
14	64.40	36.53	51.70	20.40
15	65.20	39.20	44.81	18.00
16	66.00	41.87	48.57	20.13

(b)

Experiment No.	ST1 (MPa)	ST2 (MPa)	ST3 (MPa)	SF
1	14.84	11.80	15.10	4.94
2	16.81	6.02	15.65	5.38
3	15.66	6.45	14.14	5.16
4	16.27	7.71	16.79	5.31
5	15.54	10.81	14.35	5.23
6	15.87	5.00	14.41	6.12
7	19.55	7.24	19.37	4.49
8	14.96	6.70	18.44	5.12
9	15.39	6.92	15.92	5.51
10	17.20	7.71	17.61	5.83
11	20.21	8.73	21.88	3.82
12	15.54	6.71	16.37	4.76
13	20.35	10.05	18.31	5.72
14	20.52	9.43	16.51	5.18
15	21.73	7.63	18.12	3.90
16	15.90	5.12	14.01	4.66

(c)

Exp. No.	Improvement of ST1 (%)	Improvement of ST2 (%)	Improvement of ST3 (%)	Improvement of SF (%)
1	7.26	-83.94	18.03	3.70
2	-5.08	6.16	15.07	13.05
3	2.13	-0.55	23.22	8.42
4	-1.73	-20.24	8.84	11.54
5	2.88	-68.43	22.09	9.93
6	0.81	22.06	21.77	28.61
7	-22.20	-12.82	-5.14	-5.64
8	6.49	-4.46	-0.07	7.63
9	3.77	-7.83	13.58	15.84
10	-7.49	-20.26	4.40	22.56
11	-26.34	-36.02	-18.75	-19.75
12	2.85	-4.67	11.14	0.08
13	-27.19	-56.58	0.61	20.24
14	-28.29	-47.07	10.36	8.88
15	-35.84	-18.90	1.66	-18.06
16	0.62	20.17	23.96	-2.17

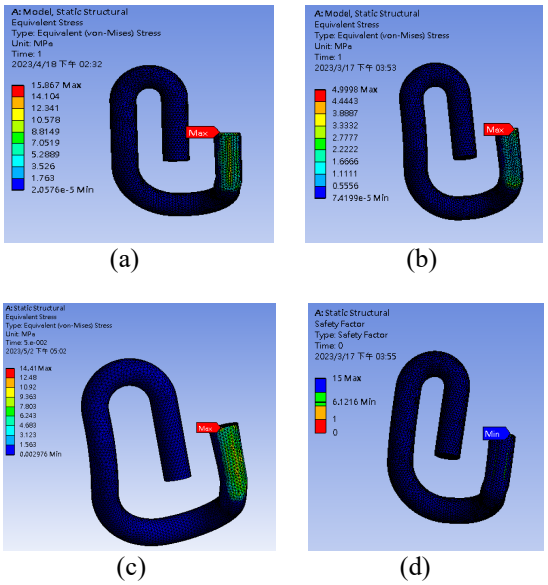

(a) (b) (c) (d)

Fig. 12 The improvement design version results for (a) EN 13146-1, (b) EN 13146-2, (c) EN 13146-3, (d) EN 13146-4 testing standards.

Optimal Design Procedure and Results

The multi-objective optimization problem is formulated as a combination of the following four

single-objective optimization problems:

$$\min_x \hat{y}_i(x),\ \ x=\{x_1,\ x_2,\ x_3,\ x_4\} \quad (16)$$
$$i=1\ \textit{for}\ \text{ST1},\ i=2\ \textit{for}\ \text{ST2},\ i=3\ \textit{for}\ \text{ST3}.$$

$$\max_x \hat{y}_i(x),\ \ x=\{x_1,\ x_2,\ x_3,\ x_4\} \quad (17)$$
$$i=4\ \textit{for}\ \text{SF}.$$

To solve the multi-objective optimization problem, this study adopts a comprehensive approach that integrates UD, KGI, GRA, EWA, and GA. KGI technique is used for creating the surrogate model and objective functions for the input and output data presented in Table 3(a). GA method is applied for the single objective optimization of each objective function. Since the problem involves four objective functions (ST1, ST2, ST3, and SF), the EWA method is employed to calculate the optimal weights (W1, W2, W3, W4) corresponding to each function. These weights are subsequently used to combine the four individual objective functions into a single composite objective function, GRD, using the GRA method. Finally, the GA method is applied again to determine the optimal solution and corresponding values for the composite objective function.

This integrated approach ensures that each analytical technique and algorithm contributes its unique strengths, enhancing the overall effectiveness of the multi-objective optimization process.

Step 1. Determine the optimal values for each single-objective function using KGI and GA.

This step involves applying KGI and GA to identify the optimal design values for each single-objective function, which serve as the basis for calculating the grey relational degree in Step 3. For the EN 13146-1, EN 13146-2, and EN 13146-3 testing standards, the optimization follows the "Smaller-the-Better" (STB) principle. For the EN 13146-4 testing standard, the "Larger-the-Better" (LTB) principle is applied. The resulting optimal values for each single-objective function are presented in Table 4.

Table 4. Optimal values for each single-objective function.

Objective function	ST1 (MPa)	ST2 (MPa)	ST3 (MPa)	SF
Optimal value	14.21	4.94	13.99	6.18

Step 2. Determine the optimal weights for the four objective functions using EWA.

This step involves applying EWA to calculate the optimal weights for the four objective functions: ST1, ST2, ST3, and SF. The EWA ensures that the weight assigned to each objective function reflects its relative importance and variability. These weights are critical for combining the individual objective functions into a single composite objective function in the subsequent step. The calculated weights are 0.2911, 0.2434, 0.2769, and 0.1887.

Step 3. Transform the values of the four objective functions into GRD using GRA

The UD findings in Table 3(b) are normalized for each objective function using the optimal values provided in Table 4. The GRD is determined using GRA described in Equations (1) to (5) and applying the optimal weights established in step 1. This process combines the four single objective functions to produce the GRD, an integrated objective function. The values for the GRD are shown in Table 5.

Table 5. Grey relation grade results

Experiment No.	GRD	Experiment No.	GRD
1	0.652	9	0.691
2	0.673	10	0.636
3	0.717	11	0.447
4	0.620	12	0.636
5	0.668	13	0.559
6	0.892	14	0.538
7	0.508	15	0.473
8	0.656	16	0.652

Step 4. Utilizing KGI and GA to determine the optimal control factor solution that maximizes GRD.

The KGI approach is utilized again to build the surrogate model for GRD. The optimal GRD and its corresponding optimal solution, in terms of control factors, are obtained using GA, as shown in Table 6.

Table 6. Optimal solution and corresponding maximal GRD.

Optimal solution (control factor)				Optimal values (Predicted value)
L1 (mm)	L2 (mm)	L3 (mm)	d (mm)	GRD
58.22	42.25	42.30	21.27	0.898

Step 5. Determine the predicted values for each objective function.

The optimal solution obtained in Step 4 is applied to determine the predicted values for each objective function. The KGS models for each objective function are utilized to perform the predictions, and the results are presented in Table 7.

Step 6. Using SolidWorks and ANSYS/Workbench to determine the actual value for each objective function

Based on the optimal solution obtained in Step 4, a redesigned rail e-clip model is created in SolidWorks software. This model is then analyzed using ANSYS/Workbench to determine the actual values for ST1, ST2, ST3, and SF under the EN 13146-1, EN 13146-2, EN 13146-3, and EN 13146-4

testing simulations. The actual values are compared with the predicted values obtained in Step 5, and the prediction errors for ST1, ST2, ST3, and SF are calculated. The results, including the actual values and their corresponding prediction errors, are presented in Table 7.

Table 7. Comparison of predicted and actual values for objective functions.

Measure	Predicted value	Actual value	Predicted Error (%)
ST1 (MPa)	14.21	14.41	1.4
ST2 (MPa)	4.94	4.99	1.0
ST3 (MPa)	13.33	13.16	1.3
SF	6.18	6.18	0.0
GRD	0.898	0.898	0.0

In Table 7, the predicted errors for ST1, ST2, ST3, and SF are all observed to be below 3%, thereby demonstrating the high level of accuracy exhibited by the surrogate models. Additionally, the GRD has been enhanced, signifying the successful accomplishment of the optimization procedure. The maximum VMS values for ST1, ST2, ST3, and the minimum SF, as determined using the optimal solutions in the redesigned version, are depicted in Figure 13.

In Table 8, we compare the maximum VMS and minimum SF values and their rates of improvement through different phases. Using the UD technique, we found the maximum VMS to be 15.87 MPa for ST1, 4.99 MPa for ST2, and 14.41 MPa for ST3. Additionally, the minimal SF for tiredness increased to 6.12. After employing multi-objective optimization, we observed a noticeable improvement. For ST1, ST2, and ST3, the maximum VMS values decreased to 14.41 MPa, 4.99 MPa, and 13.16 MPa, respectively. Additionally, the improved design demonstrates that the von Mises stress has decreased for ST1, ST2, and ST3 by 9.9%, 22.12%, and 28.6%, respectively. Likewise, the fatigue safety factor improved by 29.8% and the minimum SF increased to 6.18. These results indicate that the rail e-clip's optimal design outperforms the original design of the fastening system.

Table 8. Values and improvement in measures for different phases.

Phase	Measure	Value	Improvement (%)
Original design	ST1 (MPa)	16.00	—
	ST2 (MPa)	6.42	—
	ST3 (MPa)	18.42	
	SF	4.76	—
After uniform experiments	ST1 (MPa)	15.87	0.77
	ST2 (MPa)	4.99	22.12
	ST3 (MPa)	14.41	21.76
	SF	6.12	28.61
After multi-objective optimization	ST1 (MPa)	14.41	9.9
	ST2 (MPa)	4.99	22.12
	ST3 (MPa)	13.16	28.6
	SF	6.18	29.8

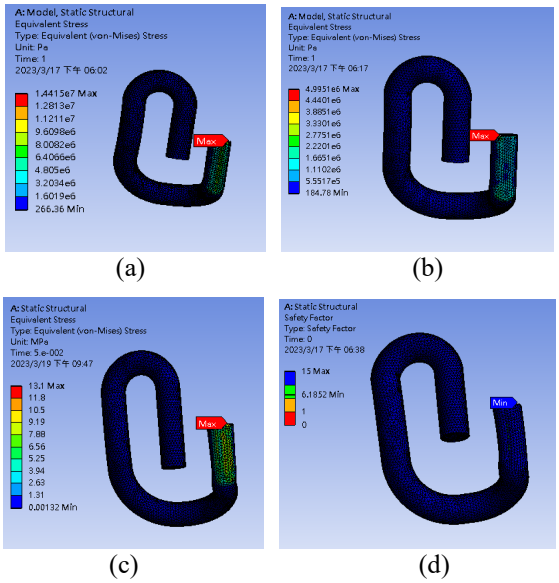

Fig. 13 The ultimate best design for test simulations for EN testing standards (a) EN 13146-1, (b) EN 13146-2, (c) EN 13146-3 and (d) EN 13146-4, includes the maximum VMS and the minimum SF.

Sensitivity Analysis

The optimization procedure aims to identify the optimal values and solutions for the rail e-clip fastening system. Additionally, the Kriging (KGS) models for ST1, ST2, ST3, SF, GRD, and the control factors have been established using Equations (11)~(15) and (17). Prior studies have not investigated the interplay between control variables and the impact of each control element on ST1, ST2, ST3, SF, and GRD. To address this gap, Sobol sensitivity analysis is employed in this study to quantify the contribution of each control factor to the variance in the system's performance metrics. Sobol sensitivity analysis (Zhang et al. 2015) is a variance-based global method that decomposes the variance of the model output into contributions from individual input variables and their interactions. This method provides a comprehensive understanding of the influence of individual factors and their interactions on the responses, including ST1, ST2, ST3, SF, and GRD. Table 9 presents the Sobol sensitivity analysis results obtained from the Kriging surrogate model for ST1, ST2, ST3, SF, and GRD. The main sensitivity represents the individual contribution of each input variable to the output variance, without considering interactions with other variables. The total sensitivity measures the total contribution of each input variable to the output variance, including both its individual effect and its interactions with other variables.

For ST1, Table 9 shows that the most significant control factors are L1, L2, and d, with d having the largest overall contribution. L3, however, has a negligible impact. For ST2, Table 9 identifies d

as the most important control factor, significantly influencing the outcome both directly and through interactions. L2 also has a strong effect, primarily due to its interactions with other factors. L3 contributes moderately, with its importance increased by interactions, while L1 has little effect and can be considered a less critical factor. For ST3, Table 9 shows that d is the most influential factor, both directly and through interactions. L2 has a strong influence, especially due to its interactions with other factors. L3 has a minor effect, while L1 is negligible and can be considered unimportant. For SF, Table 9 highlights d as the most influential control factor, both directly and through interactions. L2 is also important, largely due to its direct contribution and its interactions with other factors. L3 has a small impact, and L1 is negligible, making it an unimportant factor. Lastly, for GRD, Table 9 shows that L2 and d are the two most influential factors, both individually and through their interactions with other variables. L2 has the highest total sensitivity, indicating that its interactions play a major role in the system's behavior. d also exerts strong influence, contributing significantly to both the direct and total variance. In contrast, L1 and L3 have minimal effects and can be considered less critical.

Table 10 shows the factor influence degree table. Three asterisks (***) indicate high influence, meaning the control factor has a strong or significant effect on the outcome. Two asterisks (**) denote moderate influence, suggesting the control factor contributes noticeably but is less dominant. One asterisk (*) represents low influence, meaning the factor has a minimal effect on the result. Two hyphens (--) indicate negligible or no influence, meaning the factor does not significantly impact the response variable. L1 has no influence on most outputs, except for ST1, where it shows moderate importance. L2 is consistently influential, with moderate to high importance across all outputs, making it a significant control factor, particularly for SF and GRD. L3 has minimal influence overall, contributing slightly to ST2 but not significantly affecting the other metrics. d is a highly influential factor, with a strong effect on most outputs, especially ST2, ST3, and SF, where it shows the highest level of influence.

Table 9. Sensitivity analysis results of factors.

Sensitivity	Objective function	Control factor			
		L1 (mm)	L2 (mm)	L3 (mm)	d (mm)
Main sensitivity	ST1	0.277	0.250	0	0.256
	ST2	0.02	0.145	0.080	0.349
	ST3	0.0001	0.301	0.011	0.571
	SF	0.007	0.322	0.002	0.314
	GRD	0.025	0.568	0.0003	0.339
Total sensitivity	ST1	0.404	0.422	0.0001	0.43
	ST2	0.038	0.433	0.245	0.708
	ST3	0.0002	0.415	0.018	0.686
	SF	0.008	0.670	0.019	0.663
	GRD	0.044	0.633	0.0008	0.400

Table 10. Factor influence degree table.

Control factor	ST1	ST2	ST3	SF	GRD
L1	**	--	--	--	--
L2	**	**	**	***	***
L3	--	*	--	--	--
d	**	***	***	***	**

CONCLUSION

This study aimed to enhance the strength analysis and design of the e-clip in rail fastening systems. Finite element analysis (FEA) was performed following the EN 13146-1, EN 13146-2, and EN 13146-3 standards to evaluate the von Mises stress (VMS) distribution of the rail e-clip. Simultaneously, the fatigue safety factor (SF) was calculated based on EN 13146-4 test simulations. The uniform design of experiments (UD) methodology was employed to analyze the maximum VMS and minimum SF across various simulations, demonstrating notable improvements. Specifically, the EN 13146-1 test simulation showed a 0.77% improvement, while the EN 13146-2 and EN 13146-3 simulations yielded 22.1% and 21.7% improvements, respectively. Moreover, the EN 13146-4 test simulation significantly increased the minimum SF by 28.61%.

Optimization techniques, including the genetic algorithm (GA), entropy weighting approach (EWA), and grey relational analysis (GRA), were applied using Kriging surrogate models to determine optimal solutions for minimizing VMS and maximizing SF. As a result, the minimum SF increased to 6.18, while the maximum VMS values were reduced to 14.41 MPa, 4.99 MPa, and 13.16 MPa, respectively, indicating a significant improvement in the fatigue life of the rail e-clip. Finally, Sobol sensitivity analysis was conducted to assess the impact of design variables on the objective functions, revealing that the most influential factors affecting performance are variables d and L2.

ACKNOWLEDGMENT

Financial support for this work was provided by the National Science and Technology Council in Taiwan, R.O.C, under the contract MOST 113-2221-E-992-027.

REFERENCES

Ayşegül T. I. and Esra A. A., "The Decision-Making Approach Based on the Combination of Entropy and Rov Methods for the Apple Selection Problem," *European Journal of Interdisciplinary Studies*, Vol. 3, No. 3, pp.80-86 (2017).

Iqbal M., Prihatanto R., Aghastya A., Adi W. T. and W. Riyanta, "Inspection of Clamping Force for

E-Clip and DE Clip Fastening Systems," *Proceedings of the 2nd International Conference on Railway and Transportation 2023*, pp.459-467 (2024).

Cheng Y. C. and Wu P. H., "Optimisation for Suspension System of a Railway Vehicle with a New Non-Linear Creep Model Developed by Uniform Design," *International Journal of Heavy Vehicle Systems*, Vol. 22, No. 2, pp.157-191 (2015).

Cheng Y. C., Kuo C. M., Lee C. K. and Xie M. S., "Optimization Design of Rail Clip in Vossloh Fastening System by Uniform Design and Grey Relation Analysis," *Proceedings of the Institution of Mechanical Engineers, Part C: Journal of Mechanical Engineering Science*, Vol. 235, No. 21, pp.5639-5652 (2021).

Choi J. and Kim B., "Failure Analysis of Anchor Bolt of Rail Fastening System for Direct Fixation Track," *Engineering Failure Analysis*, Vol. 112, pp.1-14 (2020).

Deng J., "Control Problems of Grey Systems," *Systems and Control Letters*, Vol. 1, pp.288-294 (1982).

El-sayed H. M., Zohny H. N., Riad H. S. and Fayed M. N., "A Three-Dimensional Finite Element Analysis of Concrete Sleepers and Fastening Systems Subjected to Coupling Vertical and Lateral Loads," *Engineering Failure Analysis*, Vol. 122, No.105236, pp.1-14 (2021).

EN 13146:2002. Railway Applications—Track—Test Methods for Fastening Systems. 2002.

EN 13481:2012. Railway Applications. Track. Performance Requirements for Fastening Systems. 2012.

Fang K. T. and Wang Y., "*Number-Theoretic Methods in Statistics*," London: Chapman & Hall, 1994.

Fang X. J., Park Y. C., Hu J. W. and Sim H. B., "Comparison of Fatigue Performances Based on Shape Change of Rail Fastening Spring," *Applied Sciences*, Vol. 13, No. 3, pp.1770-1~1770-11 (2023).

Ferreño D., Casado J. A., Carrascal I. A., Diego S., Ruiz E., Saiz M., Sainz-Aja J. A. and Cimentada A. I., "Experimental and Fnite Element Fatigue Assessment of the Spring Clip of the SKL-1 Railway Fastening System," *Engineering Structures*, Vol. 188, pp.553-563 (2019).

Hasap A., Paitekul P., Noraphaiphipaksa N. and Kanchanomai C., "Influence of Toe Load on the Fatigue Resistance of Elastic Rail Clips," *Proceedings of the Institution of Mechanical Engineers, Part F: Journal of Rail and Rapid Transit*, Vol. 232, No. 4, pp.1078-1087 (2018).

Hong X., Xiao G., Haoyu W., Xing L. and Sixing W., "Fatigue Damage Analysis and Life Prediction of E-Clip in Railway Fasteners Based on ABAQUS and FE-SAFE," *Advances in Mechanical Engineering*, Vol. 10, No. 3, pp.1-12 (2018).

Huang Y. L. and Lin C. T., "Constructing Grey Relation Analysis Model Evaluation of Tourism Competitiveness," *Journal of Information and Optimization Sciences*, Vol. 30, No.6, pp.1129-1138 (2009).

Kim J. H., Park Y. C., Kim M. and Sim H. B., "A Fatigue Reliability Assessment for Rail Tension Clamps Based on Field Measurement Data," *Applied Sciences*, Vol. 12, No. 2, pp.624-1~624-10 (2022).

Kim S. H., Fang X. J., Park Y. C. and Sim H. B., "Evaluation of Structural Behavior and Fatigue Performance of a KR-Type Rail Clip," *Applied Sciences*, Vol. 11, No. 24, pp.12074-1~12074-11 (2021).

Liu Y., Jiang X., Li Q. and Liu H., "Failure Analysis and Fatigue Life Prediction of High-Speed Rail Clips Based on DIC Technique," *Advances in Mechanical Engineering*, Vol. 13, No. 12, pp.1-13 (2021).

McLeana P., Léger P. and Tinawi R., "Post-Processing of Finite Element Stress Fields Using Dual Kriging Based Methods for Structural Analysis of Concrete Dams," *Finite Elements in Analysis and Design*, Vol. 42, No. 6, pp.532-546 (2006).

Mohammadzadeh S., Ahadi S. and Nouri M., "Stress-Based Fatigue Reliability Analysis of the Rail Fastening Spring Clip under Traffic Loads," *Latin American Journal of Solids and Structures*, 2014; Vol. 11, No. 6, pp.993-1011 (2014).

Muthana S. A. and Ku-Mahamud K. R., "Taguchi-Grey Relational Analysis Method for Parameter Tuning of Multi-Objective Pareto Ant Colony System Algorithm," *Journal of Information and Communication Technology*, Vol. 22, No. 2, pp.149-181 (2023).

Park Y. C., An C., Sim H. B., Kim M. and Hong J. K., "Failure Analysis of Fatigue Cracking in the Tension Clamp of a Rail Fastening System," *International Journal of Steel Structures*, Vol. 19, pp.1570-1577 (2019).

Shakeri Z., Benfriha K., Zirak N. and Shirinbayan M., "Mechanical Strength and Shape Accuracy Optimization of Polyamide FFF Parts Using Grey Relational Analysis," *Scientific Reports*, Vol. 12, No. 13142, pp.1-17 (2022).

Simpson T. W. and Mistree F., "Kriging Models for Global Approximation in Simulation-Based Multidisciplinary Design Optimization," *AIAA Journal*, Vol. 39, No. 12, pp.2233-2241 (2001).

Vatansever K. and Akgűl Y., "Performance Evaluation of Websites Using Entropy and Grey Relational Analysis Methods: The Case of Airline Companies," *Decision Science Letters*,

Vol. 7, pp.119-130 (2018).
Wu R. M. X., Zhang Z., Yan W., Fan J., Gou J., Liu B., Gide E., Soar J., Shen B., Fazal-e-Hasan S., Liu Z., Zhang P., Wang P., Cui X., Peng Z. and Wang Y., "A Comparative Analysis of the Principal Component Analysis and Entropy Weight Methods to Establish the Indexing Measurement," *PLoS ONE*, Vol. 17, No. 1, pp.e0262261-1~e0262261-26 (2022).
Xiao H., Wang J. B. and Zhang Y. R., "The Fractures of E-Type Fastening Clips Used in the Subway: Theory and Experiment," *Engineering Failure Analysis*, Vol. 81, pp.57-68 (2017).
Yan Z., Shi J., Ma D., Xiao J. and Sun L., "Experimental and Numerical Analysis of the Static–Dynamic Characteristics and Vibration Fatigue Failure Mechanism of Railway Fastening Clips," *International Journal of Rail Transportation*, Vol. 12, No. 3, pp.414-436 (2024).
Zhang X. Y., Trame M. N., Lesko L. J. and Schmidt S., "Sobol Sensitivity Analysis: A Tool to Guide the Development and Evaluation of Systems Pharmacology Models," *CPT Pharmacometrics and System Pharmacology*, 2015 Vol. 4, No. 2, pp.69-79 (2015).

NOMENCLATURE

$\mathbf{A}$	alternatives matrix for entropy weighting analysis
$\mathbf{C}$	criterion matrix for entropy weighting analysis
e_j	entropy value for each index for entropy weighting analysis
$f(x)$	known regression function for Kriging interpolation
$\boldsymbol{F}$	known column vector of length n
$\boldsymbol{P}$	normalized decision matrix for entropy weighting analysis
$\boldsymbol{r}$	correlation vector for Kriging interpolation
$\mathbf{R}$	correlation matrix of Kriging interpolation
R_c	correlation function of Kriging interpolation
$R_c(\boldsymbol{x}, \boldsymbol{x}_i)$	correlation value of $\boldsymbol{x}$ and $\boldsymbol{x}_i$, $i = 1, 2, \cdots, n$
$u_i^*(j)$	normalization value of the jth output data for grey relational analysis
$u_{ob}(j)$	objective value of entity j for grey relational analysis
W_j	weight of attribute j for grey relational analysis and entropy weighting analysis
$\boldsymbol{x}$	vector formed by unknown input variables for Kriging interpolation
$\boldsymbol{x}_i$	experimental points, $i = 1, 2, \cdots, n$
$y(\boldsymbol{x})$	unknown response function to be interpolated for Kriging interpolation
$\hat{y}(\boldsymbol{x})$	Kriging surrogate model of $y(\boldsymbol{x})$
$\hat{y}_m(\boldsymbol{x})$	Kriging surrogate model of the objective function
$\boldsymbol{Y}$	known response vector for Kriging interpolation
$\mathbf{Z}$	decision matrix for entropy weighting analysis
$\hat{\beta}$	generalized least squares estimate for Kriging interpolation
$\gamma_{0i}(j)$	grey relation coefficient of entity j for grey relational analysis
Γ_{0i}	grey relational grade for a series of u_i in the grey relational analysis